

BarraCUDA: GPUs do Leak DNN Weights

Péter Horváth
Radboud University

Lukasz Chmielewski
Masaryk University

Leo Weissbart
Radboud University

Lejla Batina
Radboud University

Yuval Yarom
Ruhr University Bochum

Abstract

Over the last decade, applications of neural networks (NNs) have spread to various aspects of our lives. A large number of companies base their businesses on building products that use neural networks for tasks such as face recognition, machine translation, and self-driving cars. Much of the intellectual property underpinning these products is encoded in the exact parameters of the neural networks. Consequently, protecting these is of utmost priority to businesses. At the same time, many of these products need to operate under a strong threat model, in which the adversary has unfettered physical control of the product. In this work, we present BarraCUDA, a novel attack on general purpose Graphic Processing Units (GPUs) that can extract parameters of neural networks running on the popular Nvidia Jetson Nano device. BarraCUDA uses correlation electromagnetic analysis to recover parameters of real-world convolutional neural networks.

1 Introduction

The field of machine learning has seen an explosive increase in interest and use over the last decade. In particular, deep learning has proven to be a versatile technique that provides state-of-the-art performance for many real-world application. The use of Deep Neural Networks (DNNs) proved useful for a broad range of domains including playing chess [57], object detection [39], image classification [18, 25, 34, 38, 58], audio processing [49], forecasting [36, 52, 54, 55] and natural language processing [46]. Thus, applications of deep learning are changing many areas of our lives and have become indispensable to our everyday life.

Deep learning typically employs artificial neural networks, consisting of multiple layers of (simulated) neurons. When designing a deep learning solution for a problem, the designer first chooses the network architecture, which specifies the layers of neurons, including their sizes and types, as well as how the neurons are connected, i.e. which neurons outputs

are connected to which inputs. The designer then trains the network, selecting the weights used for each weighted sum as well as bias values that are added to the sums prior to the computation of the non-linear function.

Training a network for any non-trivial example is a resource intensive process. There is a need to curate a specialized dataset of correctly labeled samples that can be used for the training, the training process often requires days and even weeks of computation on specialized high-performance hardware, such as large quantities of graphical processing units (GPUs), and the whole process requires specialized expertise that is now in high demand. Moreover, knowledge of the internals of the model may be used for designing adversarial attacks against it [16, 59]. Thus, to protect owners' IP and to defend against potential attacks, trained models are often considered trade secrets, which should be protected from undue disclosure.

At the same time, there is a strong market incentive for pushing machine learning to edge devices such as intelligent cameras, autonomous vehicles, and drones. Consequently, trained models are being deployed under a threat model that allows adversarial physical access to devices and exposes them to side-channel attacks. Indeed, side-channel attacks against neural network implementations on CPUs have been demonstrated using both electromagnetic side-channel analysis [13] and microarchitectural attacks [63], among others. Similarly, commercial deep-learning accelerators on FPGAs have also been shown to be vulnerable to parameter extraction [24] via power-analysis. However, GPUs are the dominant hardware in the world of deep learning due to their performance and the software ecosystem that they provide to implement neural networks. The CUDA parallel computing platform allows developers to quickly and efficiently deploy DNNs on modern GPUs, whose applications has spread to many areas, from datacenters to edge computing. However, due to their complexity and inherent parallelism, side-channel attacks on GPUs are challenging. So far, attacks on GPU implementations only succeeded in recovering the network architecture, but not the parameters [17, 29, 42].

Therefore, this work focuses on the following research question:

Are proprietary implementations of neural networks on GPU vulnerable to parameter extraction using side-channel analysis?

Our Contribution

This work answers the question affirmatively. We perform a side-channel attack on an Nvidia Jetson Nano device [9], recovering the weights and biases of a real-world network. Specifically, the attack collects multiple traces with random inputs and then uses correlation electromagnetic analysis (CEMA) [14] to recover the model’s parameters from these traces. We target an implementation of convolutional neural network (CNN), one of the most commonly used type of DNN nowadays, especially in the image processing context.

To carry out the attack, we overcome several challenges.

Closed Source: Typical implementations of neural networks use the closed-source TensorRT framework [10]. Using a closed-source library limits the attacker’s knowledge of the implementation. While some past works have investigated TensorRT [29], the information is incomplete, and details relevant for our attack, such as the neuron implementation strategy, are not known. As our first contribution in this work, we perform an extensive reverse engineering of the code that TensorRT produces.

Attack Localization: A second challenge is that for an effective attack, the attacker needs to localize the attack, both spatially and temporally. To overcome this challenge, we adapt techniques from the domain of side-channel attacks on cryptography. We use a variant of Test Vector Leakage Assessment (TVLA) [56] both for finding the best physical location for placing the probe and for finding the time during the operation of the neural network in which a specific neuron is evaluated.

Big Data: Due to the level of noise that the GPU environment produces, our attack requires a large number of traces. Moreover, unlike cryptographic attacks, where the attacker typically aims to recover a relatively short key, we need to extract a large number of parameters. Processing many traces a large number of times is a resource-intensive operation. To overcome this limitation we develop a CUDA-based implementation of CEMA to execute the attack 10 times faster.

Parameter Extraction: We apply our techniques to two examples of neural networks. The first, proof-of-concept network is one-dimensional, with two layers. The second, real-world example, uses a variation of the EfficientNet [60] model. We implement both models on an industry-strength Jetson Nano device, and collect 20 million traces from each. We use our CUDA-based analysis tool, and successfully extract parameters from both layers. Overall, we require 10 days for collecting the traces and one to two days for trace alignment.

Once aligned, parameters can be extracted at a rate of one weight in six minutes. The whole process is highly parallelizable. Thus, attacks on moderate-size models are well within the capabilities of well-resourced adversaries.

Disclosure. We notified Nvidia of the found vulnerabilities, who acknowledged our findings. Nvidia recommends that users follow guidelines to prevent physical access and information leakage.

Organization. The rest of this paper is organized as follows: After providing the necessary background on side-channel attacks and on deep learning (Section 2), we describe the overview of our attack and our experiment setup in Section 3. Finally, we present our parameter extraction attack in Section 4. In addition, Section 5 covers the limitations, possible extensions, countermeasures, and related work.

2 Background

Here we introduce the concepts of side channels and related techniques that are used for the attacks and we provide some background on Nvidia’s CUDA programming model and GPU architecture.

2.1 Deep neural networks

Deep neural networks (DNN) are universal function approximators [28] that solve tasks by learning from data. First, a model learns from training data, then it can be deployed to make predictions on new, unseen data. There are two main components that influence how the trained model will perform on unseen data: the architecture and the parameters. The **architecture** refers to the structure of the model, the types and order of transformations that the model applies on its inputs to arrive at some output. These transformations are also commonly called *layers* and their output can be tweaked by changing their internal **parameters**. During the training process, these parameters are tweaked such that the final output yields correct results.

Convolutional layer. A convolutional layer consists of small *kernels* that each extract different features from the layer’s input e.g., an image. The dimensions of these kernels are usually much smaller than the input’s dimensions to be able to extract fine-grained details. Each kernel extracts different features by having its own parameters, the weights and bias. By sliding every kernel on the input with a certain step size, each of them calculates the convolution between their parameters and a small part of the input. In this work, we demonstrate the extraction of parameters, the weights and the bias, from convolutional layers.

2.2 Side-Channel Analysis

Side-Channel Analysis (SCA) exploits unintended physical leakages of electronic devices to extract secret information

processed by them [32, 33]. Such leakage can occur through various channels, including power consumption, electromagnetic emanations (EM), timing, optical or sound, and might lead to leakage of various types of secret information, e.g., on data and instructions processed. In academic settings, Side-Channel Analysis (SCA) was first introduced in the 90’s targeting cryptographic implementations running on then popular, but constrained cryptographic devices such as smart-cards [32, 33] and SCA poses ever since a constant threat to the security of various embedded systems. In that context SCA aimed to recover the secret keys used in the cryptographic implementations. In this work, we exploit the EM side channel emanating from a GPU platform on which neural network is running, but instead of targeting secret keys we show how to recover neural network secret parameters: weights and biases.

2.2.1 Electromagnetic emanation

The electromagnetic emanations from a computing device correlate with the code and the data that the device processes. This correlation has been used to break cryptographic implementations [35, 51], reverse-engineer neural networks [13, 17] and eavesdrop on display units [22, 27, 40].

In Correlation EM Analysis (CEMA) [14], the attacker uses the correlation coefficient as a side-channel distinguisher, i.e. the statistical method used for the key recovery. Essentially, CEMA allows an attacker to recover parts of a secret that is used in a targeted operation by using a known plaintext attack: measured samples are correlated against a synthetic leakage value (i.e. leakage model) that is generated from an intermediate value calculated for all possible values of a (part of) the secret. In our case all CNN parameters (i.e., weights and bias) are considered as the whole secret, and a single weight or bias are considered to be a single target of CEMA that needs to be repeated for all of them; the intermediate values are results of computations within neuron. Observe that for the above approach to work we need to assume that the inputs used in the computations are different and known to the attacker.

Two commonly used leakage models are the Hamming weight (HW) model, which predicts that the leakage is linear with the number of set bits in the data (i.e. its Hamming weight), and the Hamming distance (HD) model, which predicts that the leakage is linear with the number of bits that flip between consecutive data values. HW leakage usually occurs in practice when a value is transferred via system bus and HD leakage when an intermediate value stored in a register is overwritten with another value. We consider both of these models in this paper.

2.2.2 Leakage evaluation

For leakage evaluation, in this paper we use intermediate-value correlation and Test Vector Leakage Assessment

(TVLA) [56], which we now describe. The idea behind intermediate-value correlation is to simply look at the correlation trace generated for the correct secret value. There simply should be a peak in the place where the value desired intermediate value is processed. While this approach is closer to the real attack than TVLA or χ^2 -test, it has a disadvantage: it requires similar amount of traces as the CEMA attack; only the computational part is faster since we do not need to enumerate through all possible secret values since we control the parameters in the leakage detection phase.

The main idea of TVLA is to check whether two distributions that process different intermediate values are equivalent or not using Welch’s t -test; if such groups are deemed equivalent then the leakage is not observed by TVLA. In our setting we apply TVLA as follows: we verify whether two sets of measurements show significant difference if one set has a fixed weight and the other has random weights; we refer to this setting as fixed versus random. Note that the result of TVLA (i.e., the t -value) can be also used to determine which location of an probe is the best [20]: we can simply check at which location the absolute t -test peak is the highest.

Since TVLA searches for any leakage and not necessarily leakage exploitable by CEMA, it also usually requires less traces to collect that intermediate-value correlation or CEMA. Therefore, when applying we usually first run TVLA and then confirm the results using intermediate-value correlation.

2.3 CUDA programming model

To leverage the parallelism offered by GPUs, Nvidia exposes the CUDA programming model [6] to developers. In this model, multiple abstraction levels exist and each level has different implications with respect to the GPU hardware. The lowest level of abstraction is the `thread`, which executes a CUDA function defined by the developer. The number of threads executing the CUDA function in parallel is specified at the time of invoking the function.¹ Subsequently, multiple threads can be grouped together into a single `block` of threads. Threads in a block have a per-block on-chip shared memory region where they can exchange data with other threads in the block. Blocks of threads form a `grid` of thread blocks. Each block in a grid executes independently from other blocks, but all blocks in the grid share the same off-chip global memory region.

2.4 GPU streaming multiprocessor

When a CUDA function is invoked, the parallel threads execute on the Streaming Multiprocessor (SM) of the GPU. A GPU can consist of one or more SMs to further improve parallelism. Our target, the Jetson Nano, features a Tegra X1 System-On-Chip (SoC) that consists of one SM of the

¹Functions in CUDA are also called *kernels*. We use the term function to avoid confusion with kernels in CNNs.

Maxwell architecture [11] and CUDA Compute Capability 5.3 [3] from Nvidia. When blocks of threads are scheduled onto a particular SM, the threads in the blocks are divided into groups of 32 threads, also called *warps*. Every warp is assigned to a particular Processing Unit (PU) in the SM, and the warp scheduler in a PU is responsible for scheduling and issuing instructions for assigned warps that are ready. Additionally, an SM has 4 PUs, each with dedicated resources (e.g., register file) to manage warps.

2.5 TensorRT workflow

TensorRT is a framework dedicated to accelerate neural network inference on GPU, using implementations from different libraries (CuDNN, CuBLAS, TensorRT) that are timed against each other to choose the fastest. We use the TensorRT framework in our experiments and demonstrate the parameter extraction attack on the implementations provided by the framework.

3 Attack Procedure

This section presents our attack. It first describes the threat model and overviews the attack, before proceeding to describe the components of the attack.

3.1 Threat model

Our attack targets edge devices that execute machine learning inference for their functionality. The attacker aims to recover the trade secrets encoded in the parameters (weights and biases) of the machine learning model, for example, in order to steal the IP that encodes them or as a step in designing an adversarial attack on the machine learning model.

We assume that the target device operates correctly and that the code is secure so the attacker cannot exploit programming vulnerabilities to acquire the parameters. However, we assume that the attacker knows the architecture of the model, including the number of layers, their sizes and types, and how they interconnect. Attackers that do not have the information, can use techniques developed in past works to recover the architecture [17, 29, 42].

As is typical for edge devices, we assume that the attacker has unfettered physical access to the device. In particular, we assume that the attacker can open the device and place electromagnetic probes at locations that leak information. As we discuss in Section 3.3, there are multiple leaky location in our target device, allowing the attacker a choice.

Last, we assume that the attacker can monitor the electromagnetic emanations from the target device during the time that the device performs inference. The attacker needs to be able to observe the emanations over multiple sets of inputs and should also know what these inputs are. However, the

attacker does not require the ability to actively choose these inputs.

3.2 Attack Overview

Executing our side-channel attack consists of several phases that we describe on a high-level first and include detailed descriptions in subsequent subsections. Note that our attack assumes that the attacker has a prior knowledge of the high-level architecture of the CNN, including the number of layers and kernels, among others.

First, we built our *experimental setup* to perform the attack (see Section 3.3 for details). Since we are using EM analysis we need to find the best location for the EM probe. We performed the following tasks to find the most promising location for the probe: (1) an automated detailed XY scan over the chip surface, similarly to the work performed in [20]; (2) manual placement of the EM probe over capacitors. Overall the best location occurred to be just above the capacitor, as shown in Figure 1, but other locations above the chip surface also allowed us to extract parameters.

As mentioned in Section 2.2.2, to find the best location we first use TVLA and then we confirm the results with known-key correlation. In particular: we used TVLA with two groups that only differ with respect to the first weight: in one group it is a fixed, but randomly initialized value of -1.22 and in the other it is random. The known-key correlation was made with random weights.

Due to the jitter on the chip being heavily present we also needed to *preprocess traces* to be able to both detect and exploit the present leakage. The situation was even more challenging due to the complexity of the attacked target, including not only inherent parallelism of GPUs that is visible, but also a Linux operating system running on Quad-core ARM Cortex-A57. This results in a significant level of noise similarly to the related work Luo et al., attacking an AES implementation on a GPU platform [41]. We experimented with various preprocessing and alignment methods but eventually we used a simple static correlation based alignment. For details, about how we did the alignment and solved this challenge, see Section 3.4.

At the moment we had a working setup we also needed to analyze the attacked implementation. We *reverse engineered* the attacked GPU implementation and selected operations that are likely to leak. We also matched the operations to the traces by visual means and using correlation. We give more details in Section 3.5.

Subsequently, we needed to perform a *characterization* (see Section 3.6), namely, a preliminary analysis of the traces to investigate how to practically execute the attack. To determine on which pattern to align we used the following trial and error approach. We aligned several patterns and we used both TVLA and known-key correlation to find the best one leakage, similarly to choosing the “best EM leakage” location.



Figure 1: Location of the Langer EM probe. The probe tip is located between two capacitors. In order to access to the Tegra SoC and nearby capacitors, we removed the heatsink.

This way we learnt not only at which points the traces need alignment, but also which unique pattern in the traces correspond to which intermediate value leakage (as we eventually attack these patterns during execution of the attack - see Section 4). Moreover, we needed to analyze the traces not only with respect to the intermediate values, but also with respect to the leakage model. We used both TVLA and correlation for this purpose. Overall, we were able to find the most optimal for leakage models and alignment places.

Finally, available open-source implementations of CEMA proved to be slow for parameter extraction (1 hour CPU time to extract a single parameter). Therefore, we implemented CEMA in CUDA to improve efficiency using parallelism. This is not a novel work but since we could not find such implementation available online, we are planning to open-source our tool. For details about this step see Section 3.7.

3.3 Experimental setup

To gather side-channel information, we collect EM traces as it is less invasive and can provide more localized information than power measurements. It is also closer to real world as less modifications of the chip are required. In our setup, the Jetson Nano’s GPU cores operate at the highest possible clock frequency at 921 MHz. In order to collect electromagnetic traces, we use the Lecroy 8404M-MS oscilloscope at a sampling rate of 10GS/s with the Langer MFA-R 0.275 near-field probe [1]. Each trace contains measurements of the electromagnetic emanations of the GPU when the target neural network executes inference.

EM probe location. To find the best place for placing the EM probe, we use both TVLA and intermediate-value correlation experiments. Specifically, for each possible location we instantiate models with architecture identical to the target model, and capture two sets of traces. In the “fixed” set of traces, the model and the inputs are always the same. In the “random” set of inputs, we select a random value for one of the weights in the model. We then use TVLA to measure the statistical difference, expressed as the t -value, between

the set of traces, and intermediate-value correlation to find the correlation between the random weights and the leakage. Large correlation and t -value indicate a strong signal.

We observe several promising locations for placing the EM probe to capture the signal coming from the GPU and launch an attack. Figure 1 shows one such location, between two capacitors in the power-supply circuit of the board. Additionally, we found promising locations, exhibiting similar leakage, on the surface of the Tegra SoC itself by performing a detailed XY scan and using TVLA. We experimented with attacking at the best surface location and above the capacitors: we were able to extract parameters using each location separately. The experiments in this paper use the capacitors location since the probe placement is easier and it does not require a detailed scan.

Trace acquisition. In order to extract the parts of the traces related only to the inference operation, we used `nvprof` from the CUDA Toolkit to get information about the execution times of the operations on the GPU. Additionally, we first used GPIO pins on the board to trigger the oscilloscope to collect traces. However, this method leads to large misalignments in the collected traces because there is a high variance in the time between the trigger signal and the actual start of the inference operation on the GPU. Therefore, we used the oscilloscope’s SmartTrigger feature to trigger on the rising edge of the first layer as it proved to be more reliable.

3.4 Trace preprocessing

In general, the collected traces contain lot of jitter and the clock of the cores is not stable, which can be confirmed by looking at the traces in the frequency domain. This makes the leakage detection and the subsequent CEMA attack harder. Since accurate alignment with static alignment [43]² at many locations at the same time is not possible, we use elastic alignment [61]³ in the leakage detection process. Although elastic alignment allows us to align the traces at every time point, it requires finding the optimal input parameters and is computationally expensive. Moreover, despite tuning the alignment parameters it decreases the amount of leakage in the traces. Therefore, it is used only to align traces to detect leaking points but the CEMA attack is carried out on the raw traces after static alignment is applied on the leaky part of the trace.

²Static alignment employs a standard pattern-based approach: we select a part of a trace as a reference, and compute correlation for each offset within a chosen range for each of the traces. We then shift each trace by the respective offset that maximizes the correlation.

³Elastic alignment is a heavily-parametrized machine-learning-based technique that attempts to align the traces on all the distinctive patterns at the same time. As a result it tends to be error-prone in practice and results in a decreased leakage that is visible in TVLA results.

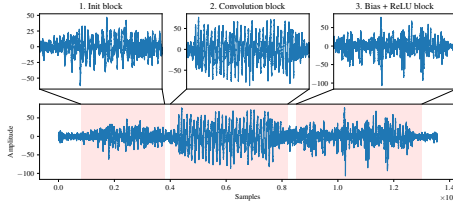


Figure 2: Segmented raw trace of first layer. The first highlighted block contains the initialization instructions. The second highlighted block is where the convolution operation is carried out. The third highlighted block corresponds to the bias addition and ReLU activation calculation.

3.5 GPU framework reverse engineering

In this subsection, we analyze the FP16 CNN implementations of the TensorRT framework on the assembly level to reverse engineer how convolution is implemented in the framework using `cuobjdump` [7]. The motivation behind analysing FP16 implementations is that during inference, latency and memory consumption are key considerations when NNs are executed. Reduced precision is an optimization technique for the NN parameters to achieve fast execution with less storage requirement. Therefore, the models are typically trained with single-precision parameters but they use reduced precision after deployment. Reduced precision techniques include binary [30], FP8 [44], INT8 [50] and FP16 [45], but the Jetson Nano has native support only for FP16.

Additionally, we match the instruction blocks of the implementations to the electromagnetic emanations of the GPU when these implementation are executed.

Implementation structure. The convolutional implementations of the framework have similar structures with the following components:

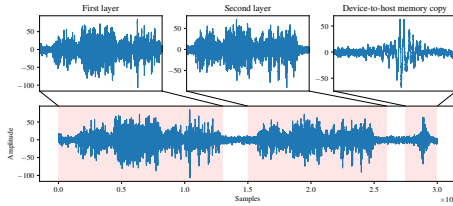


Figure 3: Raw trace of the whole operation on the GPU. The 2 layers are clearly separated in the traces. Additionally, the CUDA device-to-host memory copy is also clearly visible in the end of the trace.

- ① block of initialization instructions,
- ② block of convolution operations, and
- ③ block of bias addition and ReLU calculation.

We explain the three block in more detail as follows.

① **Init block.** The first main block consists of instructions to set up the CUDA function. In this block, 64 accumulator registers are initialized which are later used to store the convolution results. In addition, implementations make use of `half2` [5] data type in CUDA. If the `half2` data type is used, a register is packed with 2 FP16 values and the GPU can execute a floating point instruction on each half in parallel. This also introduces additional noise for SCA, in addition to the parallel threads executing in the GPU.

② **Convolutional block.** The second block carries out the convolution operation. This block consists of repeated vectorized load and half-fused-multiply-add (HFMA2) instructions. Since we use the `half2` datatype and registers are packed with two 16-bit floating point values, it is crucial to know exactly how the input data is loaded into the registers. According to the framework, the input is reformatted so that it is laid out in “*Two wide channel vectorized row major FP16 format*”. This means that each register holds inputs from two different input channels. With multiple input channels processed in parallel, our CEMA attack would then not require more time to get all the weights because the channels in the kernels are independent from each other. Additionally, the code in the second block indicates that each accumulator register is used in 8 HFMA2 instruction in this block, unless a predicated jump instruction is executed at the end of the code block which jumps back to the start of this block. This suggests that the execution of the jump instruction likely depends on the kernel size and the number of input channels of the layer.

③ **ReLU block.** The third block, repeated four times, first calculates the sum of the lower and higher half of each accumulator register. This is where the channel combinations of the convolutional operation are executed in these blocks. Then, `half2` floating point additions and `HSET` instructions are executed in the block to calculate the bias addition and the ReLU output.

Matching instruction block to the traces. Figure 2 shows a raw trace of a convolutional layer where the first highlighted section corresponds to the initialization blocks. The second highlighted block corresponds to the sum of multiplications in the convolution operation. The third highlighted segment corresponds to the calculation of the bias addition and ReLU output, repeated 4 times for different sets of registers. Note, that these instruction blocks are also separated by synchronization instructions which are also visible in the trace as the amplitude of the EM signal drops close to 0 between the blocks. Similarly, Figure 3 shows the electromagnetic emanations of the GPU during the execution of a CNN with two convolutional layers. Since each layer is mapped to a separate CUDA function call by the framework, it can be observed that there is a clear separation between layers. Additionally, the results of the convolution are copied back to memory which also a separate CUDA call and is visible in the trace.

3.6 Characterization

3.6.1 Convolutional intermediates

Establishing the time points at which intermediate values leak is a necessary step before applying CEMA. A kernel in a convolutional layer has multiple intermediate values that depend on the secret weights and the bias. A single $a \times b$ kernel with weights w , bias b and input feature map x calculates as follows:

$$c_{sum} = \mathbf{x} * \mathbf{w} = \sum_{i=1}^{a \cdot b} w_i \cdot x_i = w_1 \cdot x_1 + \dots + w_{a \cdot b} \cdot x_{a \cdot b}, \quad (1)$$

$$c_{out} = c_{sum} + b, \quad (2)$$

where c_{sum} is the result of the convolution between the weights and the input while c_{out} is the output of the kernel if the kernel contains a bias. Additionally, if there is an activation function f applied in the layer after the convolution, the final output is calculated as:

$$c_f = f(c_{out}).$$

In the above equations, c_{sum} is calculated by updating a register with the partial sums s_j of the convolution:

$$s_j = \sum_{i=1}^j w_i \cdot x_i = s_{j-1} + w_j \cdot x_j \quad (j \leq a \cdot b)$$

Therefore, the value of the register that holds s_j always depends on the previous partial sum s_{j-1} and on the product $x_i \cdot w_i$, except for the case of s_1 , where $s_0 = 0$. Since a register is updated, we use the HD leakage model to see if the update of the register from s_{j-1} to s_j leaks. In addition, we use HW on individual s_j values to establish leakage in case a bus is pre-charged with zeros before transferring data.

In order to extract every 16-bit weight separately using CEMA, all computed s_j values need to leak. If that is not the case and only the final result c_{sum} leaks, which depends on all the weights in a kernel, then the attacker needs to target all weights at once, i.e., the complexity of the attack becomes $2^{kernel_size \times 16}$ key guesses.

The solution to this problem is employing a chosen-input attack similarly to [24]. The main idea is to use an inputs with only one non-zero input feature map which causes only one component in Equation (1) to be non-zero. This requires again only 2^{16} key guesses, at the cost of stronger adversary model (i.e., the input needs to be fully controlled by the attacker) and increased number of measurements, because each weight in every layer requires a separate acquisition process.

After we recover all the weights we can compute the input to the next computations, namely c_{sum} , and to extract the bias using CEMA, either c_{out} or c_f needs to show leakage.

Weight leakage

To establish whether weight-dependent intermediates values leak, we apply random vs. fixed TVLA [23] on the partial sums s_j . However, this requires us to modify the weight on-the-fly. The TensorRT framework supports changing the weights of models, but a new CUDA context [4] has to be created every time the network's weights are changed. as per the documentation. Normally, an application is not required to create a new CUDA context for every inference operation, but it is required to be able to perform TVLA on GPU.

To detect leaky regions for each s_j , we applied TVLA separately for every weight in the target kernel. This means that in one experiment one weight in the kernel is always fixed vs.random and the rest of the weights 0. The inputs x_i are fixed throughout all the TVLA tests. This setup allows us to detect leakages corresponding to individual weights. However, false positives can be the loading of the weights.

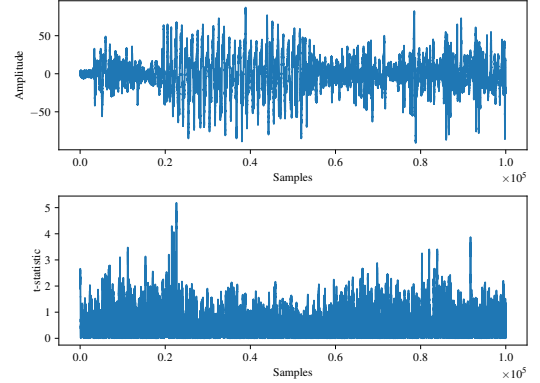


Figure 4: Result of fixed vs. random TVLA for the multiplication with the first weight in the kernel with fixed value -1.22. The top figure depicts an elastically aligned trace while the bottom figure shows the corresponding absolute t -test statistics at each time sample. There are multiple leaking spots with $|t| > 4.5$ but the overall leakage is not high.

Figure 4 shows the results of fixed vs. random TVLA for the first weight in the kernel in the first layer with 45k traces. We repeat this process for the rest of the weights and the results clearly show that leakages of the convolution operation are in the second highlighted part of Figure 2. To filter out these false positives, we also apply correlation to intermediate values. However, we also observed several ghost peaks [14, 15] with the correlation method which cannot be exploited by CEMA.

Bias leakage

Similarly, to detect leakage corresponding to the bias, we apply fixed vs. random bias TVLA and intermediate-value correlation. Similarly to the random vs. fixed weight TVLA,

the false positives in this test can be the loading of the bias.

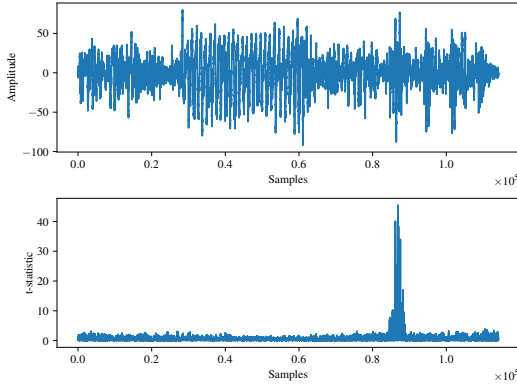


Figure 5: Result of fixed vs. random bias TVLA with fixed value 0.856. The top depicts an example trace while the bottom shows the absolute t -test statistics. There is clear leakage scattered across multiple clock cycles with $|t| > 4.5$.

Figure 5 shows the results of TVLA for the bias of the kernel in the first layer with 37k traces. There is a much clearer leakage present for the bias than for the weights in the convolution operation.

After establishing where parameters leak, with the help of elastic alignment, we use static alignment on the raw traces at these points as static alignment produced higher individual TVLA peaks as well as correlation for the attack.

3.7 CEMA implementation in CUDA

In order to calculate correlation in CEMA, covariances of populations have to be calculated that can be done with two-pass algorithms. However, for large datasets, two-pass algorithms are not efficient as the algorithm makes two iterations on the dataset. To combat this issue, one-pass algorithms have been developed to provide estimates for these statistics in large datasets [47]. In a one pass algorithm, the statistics can be updated when new data points are added to the dataset. These algorithms also make it possible to combine the statistics from subsets of the dataset to estimate the whole dataset’s statistics. This means that the statistics of each subset can be calculated in parallel, further speeding-up the CEMA attack.

However, the attack has even more aspects that can be parallelized, such as the *candidate* and *sample* levels. There are publicly available multithreaded implementations such as the JISCA library [8] for CPU, but these cannot fully parallelize the attack and become slow for large datasets.

Since we have a large number of candidates, we decided to implement CEMA for neural networks in CUDA, parallelized on three levels: dataset, candidate, sample.

Our implementation in CUDA launches a three-dimensional grid of thread blocks with dimensions: $(candidates/2, chunks, samples) = (17765, chunks, 32)$. For

our use case, the number of candidates and samples are fixed at 35530 and 32, respectively. Threads in the same warp work on the same two candidates (in parallel, due to double throughput with FP16) but correlate them with different samples. The implementation also parallelizes CEMA on a data set level, by setting *chunks* > 1. The number of chunks can vary, but setting it to 10 already gives good results in our use case with millions of traces. Depending on the GPU hardware, the optimal number may be lower or higher.

We benchmarked the multithreaded Jisca implementation on a AMD Ryzen 7950X CPU vs our CUDA implementation on a 3080 Nvidia RTX GPU. Overall, the speedup compared to JISCA is at least 5 times and typically 10 times when the dataset consists of millions of traces.

4 Parameter Extraction Results

Observe that an adversary who is able to recover a neural network’s architecture (that is our entry assumption) as well as the parameters (through our attack), can completely recovered the network model. In this section, we first demonstrate the versatility of our parameter extraction attack on a small 1-dimensional CNN and second, we mount the attack on a real-world CNN architecture by targeting the EfficientNet [60] to extract a kernel from its first two convolutional layers.

Following [13], we restrict the search space of the weights to $[-5, 5]$, as most of the parameters of trained CNNs reside in this range. To verify this, we looked at the parameters of large real-world architectures, such as [26], trained on ImageNet. With 16-bit floats, there are 35 330 possible candidates in this range. The batch size is 1 throughout the experiments.

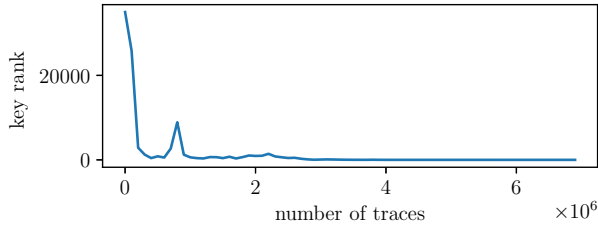
In our experiments, we recover the parameters of each architecture layer-by-layer, starting from the first layer. In the experiment, the parameters of the target architectures are initialized randomly. Observe that while we attack in an iterative fashion the trace acquisition needs to be executed only once with random known inputs. In each layer, we target the intermediate values to extract weights and biases.

4.1 Small-CNN attack

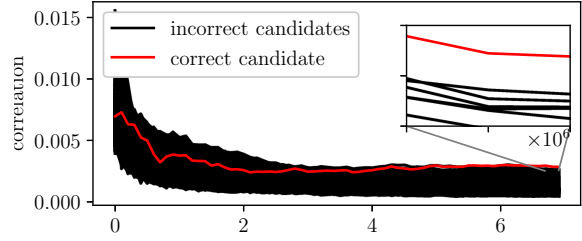
In this attack, we show how to extract the weights and the biases of a 1-dimensional CNN with 2 convolutional layers, each with one 1×5 kernel, by targeting intermediate values of the convolution computation.

Weight extraction. In this experiment, we target the intermediate values s_j (representing partial sums of the convolution between the weights of a kernel and the inputs). To extract the weights, we use HW on our chosen intermediate value, the partial sums, to map hypothetical EM consumption values to real measurements T and calculate the Pearson’s correlation per sample point between them: $\rho(HW(s_j), T)$.

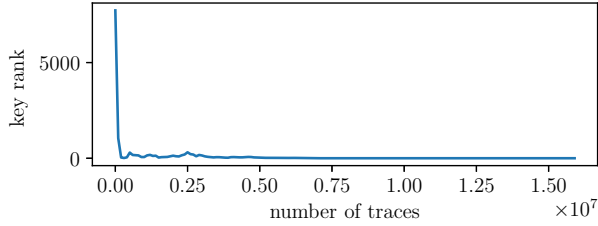
Figure 6 shows the key rankings and correlations of the correct weight value vs. the number of traces in the first layer for



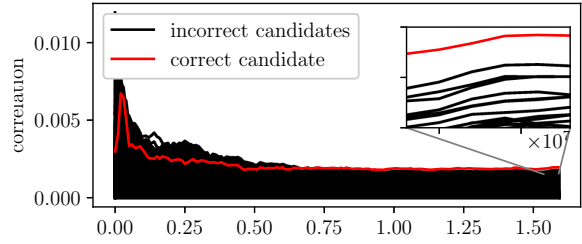
(a) Key rank vs. number of traces of the first weight in the first layer with value of -1.22.



(b) Correlation vs. number of traces (10^6) of the first weight in the first layer with value of -1.22.

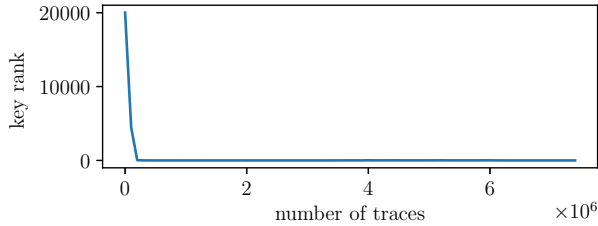


(c) Key rank vs. number of traces of the fifth weight in the first layer with value of 0.3564.

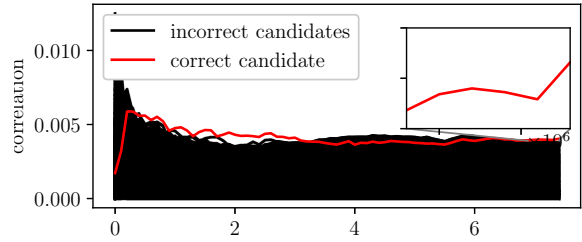


(d) Correlation vs. number of traces (10^7) of the fifth weight in the first layer with value of 0.3564.

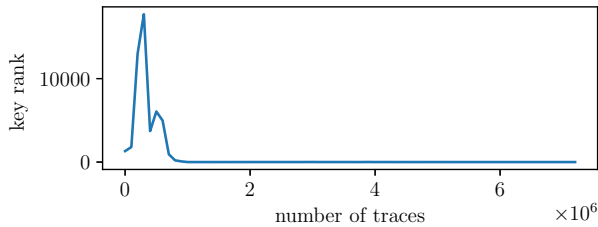
Figure 6: Key ranks and correlations of the first and fifth weights in the first layer of the small CNN architecture.



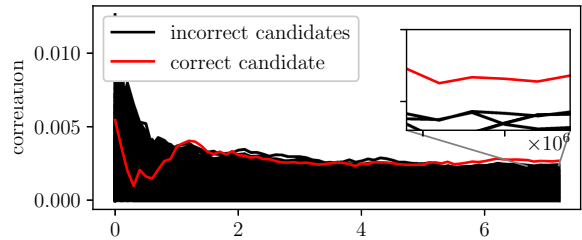
(a) Key rank vs. number of traces (10^6) of the second weight in the second layer with value of -0.5137.



(b) Correlation vs. number of traces (10^6) of the second weight in the second layer with value of -0.5137.



(c) Key rank vs. number of traces (10^6) of the third weight in the second layer with value of -0.6406.



(d) Correlation vs. number of traces (10^6) of the third weight in the second layer with value of -0.6406.

Figure 7: Key rank and correlation for the third and fourth weights in the kernel in the second layer of the small CNN architecture.

the first and fifth weights, respectively. As shown in Figure 6a, at around the 3,2 million mark, the candidate that ranks first is -1.212 for the first weight, so it is already close to the correct candidate -1.22 . At this mark, the correct candidate ranks 106th. Overall, the key rank decreases quickly but in order to get the first rank for the correct candidate, more than 5 million traces are required. Similar results are obtained for the other weights; the result for weight 5 is presented in Figure 6c.

Figure 6b shows the correlation for all the weight candidates vs. the number of traces for the first weight. As expected, it shows a similar trend to the key rank figure, as the correlation of the correct candidate gets close to the top at the 3 million traces mark. However, the correlation of the correct weight candidate only reaches the maximum after 5 million traces with respect to the incorrect candidates. Again similar results are obtained for the other weights and the result for weight 5 is presented in Figure 6d.

Figure 7 shows the key ranking and correlations of the correct weight value vs. the number of traces in the second layer, for the second and third weights; the results for the other weights are alike. Similar to the first layer, the key ranks for both weights drop quickly, but reaching a key rank of 0 requires 800 000 and 1.2 million traces for the second and third weights, respectively. Every weight in the kernel leaks similarly and targeting the partial sums can recover the correct weight candidate for all the weights in the kernel.

Although we observe correlation with *HD*, the attack with this leakage model is not successful for the small CNN.

Bias extraction. There are two operations in the convolutional layers that depend on the bias: the calculations of c_{out} and the ReLU output, $ReLU(c_{out})$. We observed two bias-related side-channel leakages that can be exploited:

1. the result of bias addition: $HW(c_{out})$,
2. the result of activation: $HW(ReLU(c_{out}))$.

We calculate the Pearson correlation for every bias candidate with these leakage models to the EM traces. Figure 9a and Figure 9b show the key rankings and correlations for the bias in the first layer. In this case, we used the ReLU intermediate to recover the bias and the key rank of the correct candidate drops rapidly but it requires a large amount of traces to fully converge to key rank 0. Figure 9c and Figure 9d show the key rankings and correlations for the bias in the second layer. In this case, we demonstrate the extraction of the bias using the $HW(c_{sum})$ intermediate showing that the ReLU nonlinearity is not required to recover the bias.

4.2 Real-world CNN attack

In this experiment, we show that our attack extends to real-world CNN by successfully extracting parameters from the first 2 convolutional layers of the EfficientNet [60] architecture.⁴ These two layers have $32 \times 3 \times 3$ kernels each.

⁴The convolutional layers in this architecture do not have biases. Therefore, we alter the architecture so that the first layer has biases in the kernels

The challenge arises from the fact that larger architectures compute more intermediate values at the same time, adding more noise to the traces. Interestingly, we are able to use both HW and HD to recover weights and biases from the layers.

Weight extraction. Again, we target the intermediate results s_j of the 2D convolution to extract the weights. In this case, we are also able to extract weights using the *HD* leakage model. As shown in Figure 8a and Figure 8b, HW also works for the larger architecture: we successfully recover the third weight of a kernel in the first layer. For the second layer, Figure 8e and Figure 8f show the key ranking and correlation for the second weight in the second layer. In addition, Figure 8g and Figure 8h show the key ranking and correlation for the third weight in the second layer demonstrating that our attack extends to larger layers as well. Overall, the convergence behavior for HW is similar to the behavior seen for the small CNN and the results are similar also for other weights.

The $HD(s_{j-1}, s_j)$ leakage model targeting a register update can also be exploited to recover weights: Figure 8c and Figure 8d show the key rankings and correlations for 9th weight in the first layer of the large architecture using HD. The attack works similarly for the other weights. As shown in Figure 8c, the convergence behavior for HD is different than for HW as it starts to converge slower. Typically, there are two kinds of errors that slow down the convergence: incorrect bit in either the exponent or the mantissa. An error in the mantissa leads to similar values to that of the true value of the target weight while an error in the exponent yields quite different values.

Bias extraction. For the real-world CNN, we are also able to use *HD* leakage model to extract the bias: we targeted the register update from c_{sum} to c_{out} : $HD(c_{sum}, c_{out})$. Figure 9e and Figure 9f show the results for the bias in the first layer of the real-world architecture. The key rank drops quickly and converges to key rank 0 in 5 million traces. Surprisingly, recovering the bias in the real-world architecture required significantly less traces than in the small architecture. We are not sure what is the reason for this situation, besides the fact the implementation is slightly different.

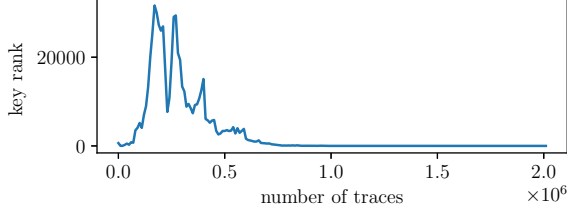
Overall, there is a large variance in the number of required traces to recover individual weights and biases, but an upper bound of 20 million traces proves to be sufficient in our experiments. In addition, the real-world CNN architecture does not require more traces to recover the parameters.

5 Discussion

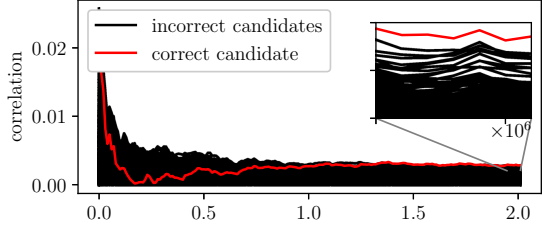
5.1 Chosen-input attack

A stronger adversary might be able to not only observe the inputs received by the target network, but also control them. This opens up an opportunity for a *chosen-input* attack [24]. In this attack, the adversary strategically sets inputs to 0 so that

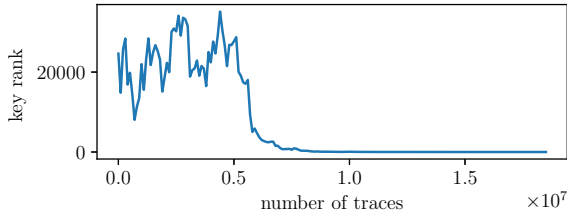
to demonstrate the bias extraction on this architecture as well.



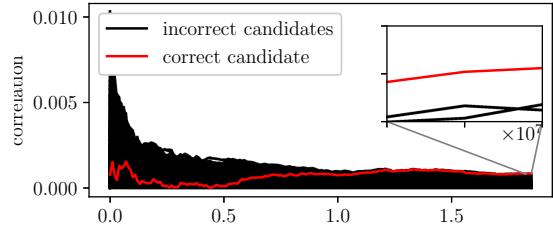
(a) Key rank vs. number of traces using *HW* for the third weight in the first layer with value of 0.8223.



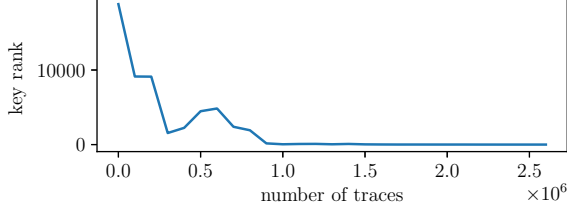
(b) Correlation vs. number of traces (10^6) using *HW* for the third weight in the first layer with value of 0.8223.



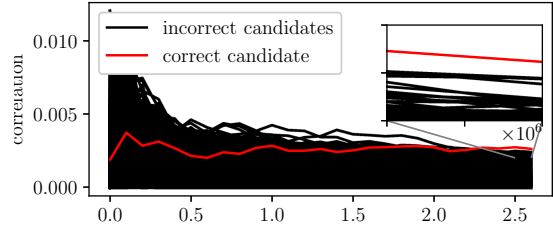
(c) Key rank vs. number of traces using *HD* for the ninth weight in the first layer with value of -0.7705.



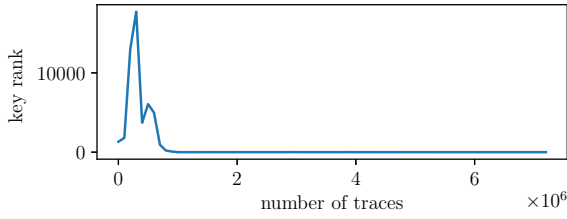
(d) Correlation vs. number of traces (10^7) using *HD* for the ninth weight in the first layer with value of -0.7705.



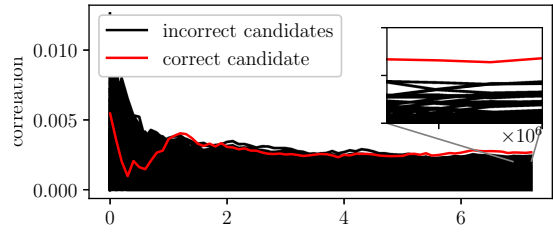
(e) Key rank vs. number of traces for s_j for the second weight in the second layer with the value of -0.5137.



(f) Correlation vs. number of traces (10^6) for s_j for the second weight in the second layer with the value of -0.5137.



(g) Key rank vs. number of traces for s_j for the third weight in the second layer with the value of -0.6406.



(h) Correlation vs. number of traces (10^6) for s_j for the third weight in the second layer with the value of -0.6406.

Figure 8: Key ranks and correlations of the different weights in the first and second layer in the real-world CNN architecture.

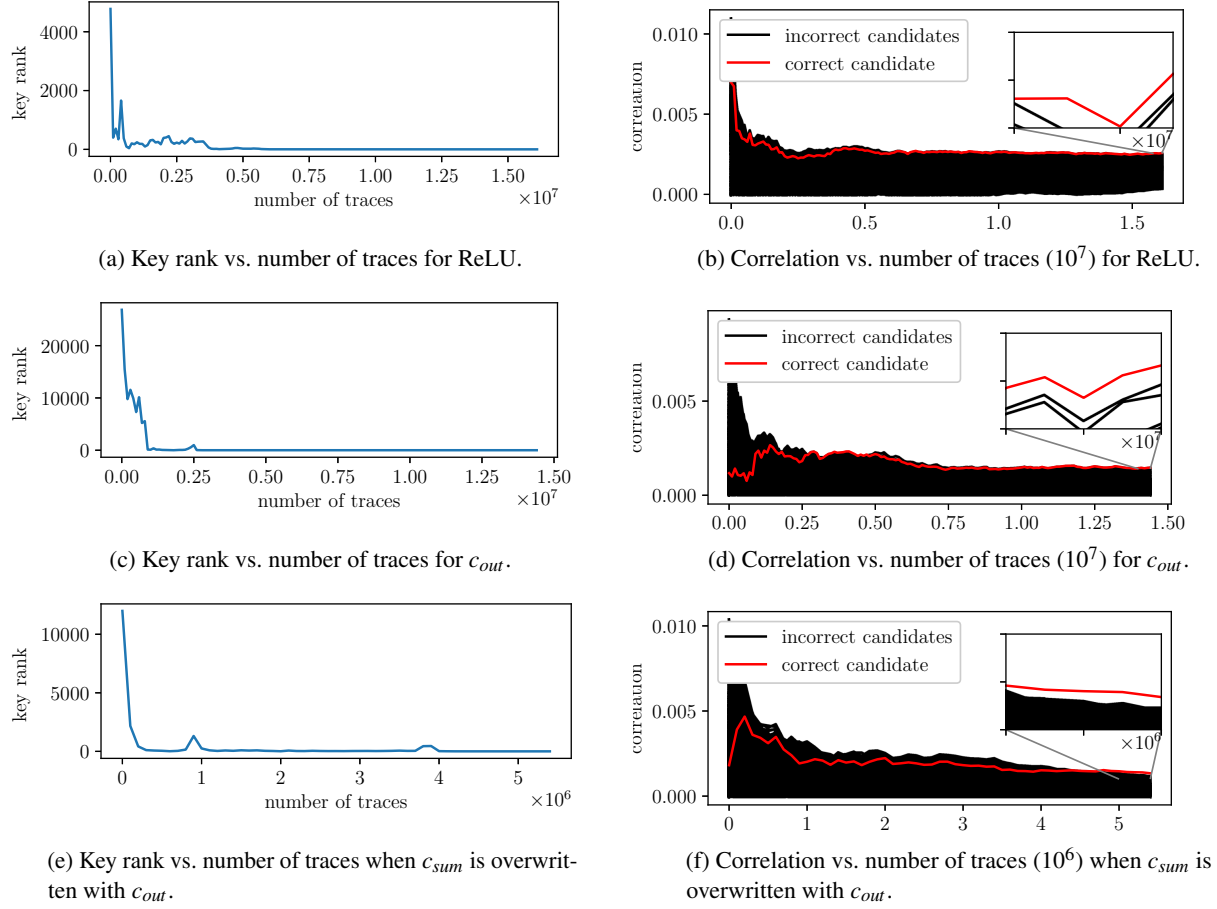


Figure 9: Key ranks and correlations of the biases with different leakage models and intermediates.

c_{sum} depends only on one weight from the kernel. Targeting the first layer with this attack is trivial, assuming the attacker controls the input. For inner layers there is a need to find inputs that induce zero values, which may be more complex.

We have executed this attack and we discovered that a single weight can be recovered with less traces than for our attack. However, the traces cannot be reused for all weights (i.e., new traces need to be collected for each weight), so the attack becomes infeasible for large models.

5.2 Desktop/Datacenter GPUs

Against large GPUs, our attack can be extended and is likely to be more expensive depending on the target neural network’s size. One key difference between the GPU in the Jetson Nano and desktop/datacenter GPUs is the number of streaming multiprocessors. Ideally, for a large GPU, an attacker would first locate all the SMs of the target GPU. Afterwards, each SM could be scanned with an EM probe to see if there’s any activity of interest. If the target neural network is extremely large and saturates all the SMs during inference, multiple

probes may be used to cover all of them and collect traces in parallel for each SM. Therefore, the equipment and overall cost is higher the more SMs of the target GPU has.

5.3 Limitations

While we experimented with two CNNs, coverage is still limited. Several aspects of the design could impact our attack:

Batch size. In our experiments, the batch size is set to 1. A larger size might cause operations with the same weights or biases to be carried out in parallel with different inputs. This means that two or more intermediates might depend on the same weight or bias at the same time. However, this should not impact our attack since it only would need to be adjusted to consider a combination of multiple intermediate values.

Concurrent applications. GPUs are able to handle and schedule concurrently CUDA functions from multiple applications. This might introduce noise, but it depends on the required resources for each CUDA function. If a CUDA function takes up most of the GPU resources (e.g. shared memory, registers, etc.), then a different CUDA function will only be

Author	Platform	clock freq. (MHz)	Side channel	Precision (bits)
Batina, et al. [13]	microcontroller	20, 84	EM	8-, 32
Dubet, et al. [21]	FPGA	24	Power	1
Yoshida, et al. [66]	FPGA	25	Power	8
Regazzoni, et al. [53]	FPGA	N/A ⁵	EM	1
Yli-Mäyry, et al. [64]	FPGA	N/A ⁵	EM	1
Li, et al. [37]	FPGA	25	Power	8
Joud, et al. [31]	microcontroller	100	EM	32
Gongye et al. [24]	FPGA	320	EM	8
BarraCUDA	GPU	920	EM	16

Table 1: Comparison with related work.

scheduled after all the thread blocks in the previous CUDA function finished execution [2]. Since larger layers are executed with 128 threads, concurrent applications would not be able to be executed at the same time as the Jetson Nano’s GPU is limited to 128 cores. Concurrency is more realistic for larger GPUs but isolating individual SMs might be sufficient to overcome the noise coming from concurrent applications.

5.4 Mitigation

Traditional ways to contain electromagnetic emanation, such as proper shielding or introducing noise to decrease the Signal-to-Noise ratio, could alleviate the problem [43]. Specifically against parameter extraction, one of the possible countermeasures, which is also mentioned in the CSI-NN paper [13], is shuffling [62] the order of multiplications in the layers, which can make it significantly harder for an adversary to recover the weights. Additionally, masking [19, 48] can also decouple the side-channel measurements and the processed data. However, this comes at the price of execution speed, which might not be desired in real-time systems. Specifically for convolution, the registers containing the results of the partial sums can be initialized with the bias of the kernel instead of initializing them with zeros. This would prompt an adversary to mount a CPA attack where the correct $b + w_1$ pair has to be recovered first. The complexity of this attack would be 32 bits due to 16 bits of complexity for the weight and bias separately.

5.5 Comparison with related work

To the best of our knowledge, no previous work has been able to extract the parameters of neural networks on GPU using physical side-channel. Previous works have demonstrated parameter extraction on microcontrollers and FPGAs using power or EM side channel, as shown in Table 1. In addition, these attacks were performed on neural networks with binary parameters [21, 53, 65], 8-bit parameters [13, 24, 37, 66] or

32-bit parameters [13, 31]. Our work demonstrates parameter extraction on 16-bit parameters with discussion on extension to 32-bit parameters. Additionally, the approach presented in this work is scalable because it does not rely on chosen inputs as in [24]. Chosen inputs are not scalable to large neural networks as crafting chosen inputs becomes harder the deeper the target NN is. Furthermore, our work presents a CEMA attack on weights where the number of cores and the clock frequency these cores operate at are significantly larger than in related works. The large number of cores, with almost 1GHz clock frequency, present a challenge in both the measurement and attack stages. Still, GPUs dominate the world of AI so it is of utmost importance to assess the resilience of GPU accelerated workloads against weight extraction attacks.

6 Conclusions

In this work, we analyzed the Nvidia Jetson Nano GPU, a commonly chosen platform for real-world neural network implementations, for resilience against side-channel attacks that aim to extract the weights of the target NN. First, we find multiple vulnerable points where the GPU leaks information about the parameters of the target DNN. Subsequently, we demonstrate the extraction of weights and biases of different CNN architectures. Overall, the neural network implementations of Nvidia’s TensorRT framework are vulnerable to parameter extraction using EM side-channel attack despite the networks running in a highly parallel and noisy environment. It remains an open problem to protect their implementations in security or privacy-sensitive applications.

References

- [1] <https://www.langer-emv.de/en/product/mfa-active-1mhz-up-to-6-ghz/32/mfa-r-0-2-75-near-field-micro-probe-1-mhz-up-to-1-ghz/854>. Accessed: 2022-01-25.

⁵The clock frequency is not disclosed in these attacks but it is at most 800MHz as both attack XILINX ZYNQ chip [12].

- [2] <https://developer.download.nvidia.com/CUDA/training/StreamsAndConcurrencyWebinar.pdf>. Accessed: 2022-11-30.
- [3] Cuda Compute Capabilities. <https://docs.nvidia.com/cuda/cuda-c-programming-guide/index.html#compute-capabilities>. Accessed: 2022-09-30.
- [4] Cuda Context. <https://docs.nvidia.com/cuda/cuda-c-programming-guide/index.html#context>. Accessed: 2022-09-30.
- [5] CUDA half2 data type. https://docs.nvidia.com/cuda/cuda-math-api/struct___half2.html#struct___half2. Accessed: 2022-09-30.
- [6] CUDA programming model. <https://docs.nvidia.com/cuda/cuda-c-programming-guide/index.html#programming-model>. Accessed: 2022-09-30.
- [7] cuobjdump. <https://docs.nvidia.com/cuda/cuda-binary-utilities/#usage>. Accessed: 2022-09-30.
- [8] Jlsca. <https://github.com/Riscure/Jlsca>. Accessed: 2022-09-30.
- [9] NVIDIA Jetson Nano. <https://developer.nvidia.com/embedded/jetson-nano-developer-kit>. Accessed: 2022-09-30.
- [10] Nvidia TensorRT. <https://developer.nvidia.com/tensorrt>. Accessed: 2022-09-30.
- [11] Tegra X1 System-On-Chip. <http://international.download.nvidia.com/pdf/tegra/Tegra-X1-whitepaper-v1.0.pdf>. Accessed: 2022-09-30.
- [12] ZYNQ Data Sheet. <https://docs.xilinx.com/v/u/en-US/ds187-XC7Z010-XC7Z020-Data-Sheet>. Accessed: 2022-09-30.
- [13] Lejla Batina, Shivam Bhasin, Dirmanto Jap, and Stjepan Picek. CSI-NN: Reverse engineering of neural network architectures through electromagnetic side channel. In *28th USENIX Security Symposium USENIX Security 19*, pages 515–532, 2019.
- [14] Eric Brier, Christophe Clavier, and Francis Olivier. Correlation power analysis with a leakage model. In *International workshop on cryptographic hardware and embedded systems*, pages 16–29. Springer, 2004.
- [15] Cécile Canovas and Jessy Clédière. What do s-boxes say in differential side channel attacks? *Cryptology ePrint Archive*, 2005.
- [16] N. Carlini and D. Wagner. Towards evaluating the robustness of neural networks. In *2017 IEEE Symposium on Security and Privacy (SP)*, pages 39–57, Los Alamitos, CA, USA, may 2017. IEEE Computer Society.
- [17] Łukasz Chmielewski and Léo Weissbart. On reverse engineering neural network implementation on GPU. In *International Conference on Applied Cryptography and Network Security*, pages 96–113. Springer, 2021.
- [18] François Chollet. Xception: Deep learning with depth-wise separable convolutions. In *Proceedings of the IEEE conference on computer vision and pattern recognition*, pages 1251–1258, 2017.
- [19] Jean-Sébastien Coron and Louis Goubin. On boolean and arithmetic masking against differential power analysis. In *Cryptographic Hardware and Embedded Systems—CHES 2000: Second International Workshop Worcester, MA, USA, August 17–18, 2000 Proceedings 2*, pages 231–237. Springer, 2000.
- [20] Josef Danial, Debayan Das, Santosh K. Ghosh, Arijit Raychowdhury, and Shreyas Sen. Sniffer: Low-cost, automated, efficient electromagnetic side-channel sniffing. *IEEE Access*, 8:173414–173427, 2019.
- [21] Anuj Dubey, Rosario Cammarota, and Aydin Aysu. Maskednet: The first hardware inference engine aiming power side-channel protection. In *IEEE International Symposium on Hardware Oriented Security and Trust*, pages 197–208, 2020.
- [22] Fırkan Elibol, Uğur Sarac, and Işin Erer. Realistic eavesdropping attacks on computer displays with low-cost and mobile receiver system. In *2012 Proceedings of the 20th European Signal Processing Conference (EUSIPCO)*, pages 1767–1771. IEEE, 2012.
- [23] Benjamin Jun Gilbert Goodwill, Josh Jaffe, Pankaj Rohatgi, et al. A testing methodology for side-channel resistance validation. In *NIST non-invasive attack testing workshop*, volume 7, pages 115–136, 2011.
- [24] Cheng Gongye, Yukui Luo, Xiaolin Xu, and Yunsu Fei. Side-channel-assisted reverse-engineering of encrypted dnn hardware accelerator ip and attack surface exploration. In *IEEE Symposium on Security and Privacy*, 2024.
- [25] Kaiming He, Xiangyu Zhang, Shaoqing Ren, and Jian Sun. Deep residual learning for image recognition. In *Proceedings of the IEEE conference on computer vision and pattern recognition*, pages 770–778, 2016.
- [26] Kaiming He, Xiangyu Zhang, Shaoqing Ren, and Jian Sun. Deep residual learning for image recognition. In *IEEE Conference on Computer Vision and Pattern Recognition*, 2016.

- [27] Zhang Hongxin, Huang Yuewang, Wang Jianxin, Lu Yinghua, and Zhang Jinling. Recognition of electromagnetic leakage information from computer radiation with SVM. *Computers & Security*, 28(1-2):72–76, 2009.
- [28] Kurt Hornik, Maxwell Stinchcombe, and Halbert White. Multilayer feedforward networks are universal approximators. *Neural Networks*, 2(5):359–366, 1989.
- [29] Peter Horvath, Lukasz Chmielewski, Leo Weissbart, Lejla Batina, and Yuval Yarom. CNN architecture extraction on edge GPU. In *Applied Cryptography and Network Security Workshops*. Springer, 2024.
- [30] Itay Hubara, Matthieu Courbariaux, Daniel Soudry, Ran El-Yaniv, and Yoshua Bengio. Binarized neural networks. In D. Lee, M. Sugiyama, U. Luxburg, I. Guyon, and R. Garnett, editors, *Advances in Neural Information Processing Systems*, volume 29. Curran Associates, Inc., 2016.
- [31] Raphaël Joud, Pierre-Alain Moëllic, Simon Pontié, and Jean-Baptiste Rigaud. A practical introduction to side-channel extraction of deep neural network parameters. In *International Conference on Smart Card Research and Advanced Applications*, pages 45–65. Springer, 2022.
- [32] Paul Kocher, Joshua Jaffe, and Benjamin Jun. Differential power analysis. In *Annual international cryptology conference*, pages 388–397. Springer, 1999.
- [33] Paul C Kocher. Timing attacks on implementations of Diffie-Hellman, RSA, DSS, and other systems. In *Annual International Cryptology Conference*, pages 104–113. Springer, 1996.
- [34] Alex Krizhevsky, Ilya Sutskever, and Geoffrey E Hinton. Imagenet classification with deep convolutional neural networks. *Advances in neural information processing systems*, 25:1097–1105, 2012.
- [35] Markus G Kuhn and Ross J Anderson. Soft tempest: Hidden data transmission using electromagnetic emanations. In *International Workshop on Information Hiding*, pages 124–142. Springer, 1998.
- [36] Nikolay Laptev, Jason Yosinski, Li Erran Li, and Slawek Smyl. Time-series extreme event forecasting with neural networks at uber. In *International conference on machine learning*, volume 34, pages 1–5. sn, 2017.
- [37] Ge Li, Mohit Tiwari, and Michael Orshansky. Power-based attacks on spatial dnn accelerators. *ACM Journal on Emerging Technologies in Computing Systems*, 18(3):1–18, 2022.
- [38] Min Lin, Qiang Chen, and Shuicheng Yan. Network in network. *arXiv preprint arXiv:1312.4400*, 2013.
- [39] Li Liu, Wanli Ouyang, Xiaogang Wang, Paul Fieguth, Jie Chen, Xinwang Liu, and Matti Pietikäinen. Deep learning for generic object detection: A survey. *International journal of computer vision*, 128(2):261–318, 2020.
- [40] Zhuoran Liu, Niels Samwel, Léo Weissbart, Zhengyu Zhao, Dirk Lauret, Lejla Batina, and Martha Larson. Screen gleaning: A screen reading tempest attack on mobile devices exploiting an electromagnetic side channel. *Network and Distributed System Security Symposium*, 2021.
- [41] Chao Luo, Yunsu Fei, Pei Luo, Saoni Mukherjee, and David Kaeli. Side-channel power analysis of a GPU AES implementation. In *2015 33rd IEEE International Conference on Computer Design (ICCD)*, pages 281–288, 2015.
- [42] Henrique Teles Maia, Chang Xiao, Dingzeyu Li, Eitan Grinspun, and Changxi Zheng. Can one hear the shape of a neural network?: Snooping the GPU via magnetic side channel. In Kevin R. B. Butler and Kurt Thomas, editors, *31st USENIX Security Symposium, USENIX Security 2022, Boston, MA, USA, August 10-12, 2022*, pages 4383–4400. USENIX Association, 2022.
- [43] Stefan Mangard, Elisabeth Oswald, and Thomas Popp. *Power analysis attacks: Revealing the secrets of smart cards*, volume 31. Springer Science & Business Media, 2008.
- [44] Paulius Micikevicius, Dusan Stolic, Neil Burgess, Marius Cornea, Pradeep Dubey, Richard Grisenthwaite, Sangwon Ha, Alexander Heinecke, Patrick Judd, John Kamalu, Naveen Mellempudi, Stuart Oberman, Mohammad Shoenybi, Michael Siu, and Hao Wu. Fp8 formats for deep learning, 2022.
- [45] Sharan Narang, Gregory Diamos, Erich Elsen, Paulius Micikevicius, Jonah Alben, David Garcia, Boris Ginsburg, Michael Houston, Oleksii Kuchaiev, Ganesh Venkatesh, et al. Mixed precision training. In *Int. Conf. on Learning Representation*, 2017.
- [46] Daniel W Otter, Julian R Medina, and Jugal K Kalita. A survey of the usages of deep learning for natural language processing. *IEEE transactions on neural networks and learning systems*, 32(2):604–624, 2020.
- [47] Philippe Pierre Pebay. Formulas for robust, one-pass parallel computation of covariances and arbitrary-order statistical moments. 9 2008.

- [48] Emmanuel Prouff and Matthieu Rivain. Masking against side-channel attacks: A formal security proof. In *Advances in Cryptology–EUROCRYPT 2013: 32nd Annual International Conference on the Theory and Applications of Cryptographic Techniques, Athens, Greece, May 26-30, 2013. Proceedings 32*, pages 142–159. Springer, 2013.
- [49] Hendrik Purwins, Bo Li, Tuomas Virtanen, Jan Schlüter, Shuo-Yiin Chang, and Tara Sainath. Deep learning for audio signal processing. *IEEE Journal of Selected Topics in Signal Processing*, 13(2):206–219, 2019.
- [50] Jerry Quinn and Miguel Ballesteros. Pieces of eight: 8-bit neural machine translation. In Srinivas Bangalore, Jennifer Chu-Carroll, and Yunyao Li, editors, *Proceedings of the 2018 Conference of the North American Chapter of the Association for Computational Linguistics: Human Language Technologies, Volume 3 (Industry Papers)*, pages 114–120, New Orleans - Louisiana, June 2018. Association for Computational Linguistics.
- [51] J.-J. Quisquater and D. Samyde. ElectroMagnetic Analysis (EMA): Measures and Counter-Measures for Smart Cards. In I. Attali and T. P. Jensen, editors, *Smart Card Programming and Security (E-smart 2001)*, volume 2140 of *Lecture Notes in Computer Science*, pages 200–210. Springer-Verlag, 2001.
- [52] Syama Sundar Rangapuram, Matthias W Seeger, Jan Gasthaus, Lorenzo Stella, Yuyang Wang, and Tim Januschowski. Deep state space models for time series forecasting. *Advances in neural information processing systems*, 31, 2018.
- [53] Francesco Regazzoni, Shivam Bhasin, Amir Ali Pour, Ihab Alshaer, Furkan Aydin, Aydin Aysu, Vincent Beroulle, Giorgio Di Natale, Paul Franzon, David Hely, et al. Machine learning and hardware security: Challenges and opportunities. In *International Conference on Computer-Aided Design*, pages 1–6, 2020.
- [54] Alaa Sagheer and Mostafa Kotb. Time series forecasting of petroleum production using deep lstm recurrent networks. *Neurocomputing*, 323:203–213, 2019.
- [55] David Salinas, Valentin Flunkert, Jan Gasthaus, and Tim Januschowski. Deepar: Probabilistic forecasting with autoregressive recurrent networks. *International Journal of Forecasting*, 36(3):1181–1191, 2020.
- [56] Tobias Schneider and Amir Moradi. Leakage assessment methodology. In *International Workshop on Cryptographic Hardware and Embedded Systems*, pages 495–513. Springer, 2015.
- [57] David Silver, Thomas Hubert, Julian Schrittwieser, Ioannis Antonoglou, Matthew Lai, Arthur Guez, Marc Lanctot, Laurent Sifre, Dhharshan Kumaran, Thore Graepel, et al. Mastering chess and shogi by self-play with a general reinforcement learning algorithm. *arXiv preprint arXiv:1712.01815*, 2017.
- [58] Karen Simonyan and Andrew Zisserman. Very deep convolutional networks for large-scale image recognition. *arXiv preprint arXiv:1409.1556*, 2014.
- [59] Christian Szegedy, Wojciech Zaremba, Ilya Sutskever, Joan Bruna, Dumitru Erhan, Ian J. Goodfellow, and Rob Fergus. Intriguing properties of neural networks. In Yoshua Bengio and Yann LeCun, editors, *2nd International Conference on Learning Representations, ICLR 2014, Banff, AB, Canada, April 14-16, 2014, Conference Track Proceedings*, 2014.
- [60] Mingxing Tan and Quoc Le. Efficientnet: Rethinking model scaling for convolutional neural networks. In *International conference on machine learning*, pages 6105–6114. PMLR, 2019.
- [61] Jasper GJ van Woudenberg, Marc F Witteman, and Bram Bakker. Improving differential power analysis by elastic alignment. In *Topics in Cryptology–CT-RSA 2011: The Cryptographers’ Track at the RSA Conference 2011, San Francisco, CA, USA, February 14-18, 2011. Proceedings*, pages 104–119. Springer, 2011.
- [62] Nicolas Veyrat-Charvillon, Marcel Medwed, Stéphanie Kerckhof, and François-Xavier Standaert. Shuffling against side-channel attacks: A comprehensive study with cautionary note. In *Advances in Cryptology–ASIACRYPT 2012: 18th International Conference on the Theory and Application of Cryptology and Information Security, Beijing, China, December 2-6, 2012. Proceedings 18*, pages 740–757. Springer, 2012.
- [63] Mengjia Yan, Christopher W. Fletcher, and Josep Torrellas. Cache telepathy: Leveraging shared resource attacks to learn DNN architectures. In *USENIX Security*, pages 2003–2020, 2020.
- [64] Ville Yli-Mäyry, Akira Ito, Naofumi Homma, Shivam Bhasin, and Dirmanto Jap. Extraction of binarized neural network architecture and secret parameters using side-channel information. In *IEEE International Symposium on Circuits and Systems, ISCAS 2021, Daegu, South Korea, May 22-28, 2021*, pages 1–5. IEEE, 2021.
- [65] Ville Yli-Mäyry, Akira Ito, Naofumi Homma, Shivam Bhasin, and Dirmanto Jap. Extraction of binarized neural network architecture and secret parameters using side-channel information. In *IEEE International Symposium on Circuits and Systems (ISCAS)*, pages 1–5, 2021.

- [66] Kota Yoshida, Takaya Kubota, Shunsuke Okura, Mitsuru Shiozaki, and Takeshi Fujino. Model reverse-engineering attack using correlation power analysis against systolic array based neural network accelerator. In *IEEE International Symposium on Circuits and Systems (ISCAS)*, pages 1–5, 2020.